Results in Engineering 32 (2026) 112198

Contents lists available at ScienceDirect

Results in Engineering

journal homepage: www.sciencedirect.com/journal/results-in-engineering

Research paper

Conjugate heat transfer and natural convection analysis of concrete bricks with varied cavity architectures: A numerical investigation of symmetric and asymmetric designs in hot climates

Hayder Al-lami [a,*], Hussain Madhi [a], Dheyaa S.J. Al-Saedi [a], Ali A.H. AlMaidi [b], Mushtaq A. Al-Furaiji [a]

[a] College of Engineering, University of Misan, Al Amarah city, Maysan, 62001, Iraq
[b] College of Agriculture, University of Misan, Al Amarah city, Misan, 62001, Iraq

ARTICLE INFO

Keywords:
Hollow concrete bricks
Passive cooling
Conjugate heat transfer
Energy saving
CFD
Thermal performance
Geometric optimization

ABSTRACT

This research investigates the thermal efficiency of concrete bricks in the extreme-arid climate by optimising internal cavity shapes. The novelty of this study lies in isolating geometric impacts from total air volume by maintaining a highly controlled constant void ratio of 13%. The research employed 3D numerical simulations in ANSYS Fluent to assess conjugate heat transfer (integrating conduction, natural convection, and radiation) across eight unconventional cavity designs and a solid reference brick under high-summer conditions in Amarah, Iraq. The findings demonstrate that internal architecture is the principal factor influencing thermal damping. The asymmetric Tilted Parallelogram brick (B_{TP}) was determined to be the superior design. By breaking direct thermal bridges, the (B_{TP}) achieved a maximum R-value of 0.063 m^2·K/W at 1 PM, representing a 96.87% improvement over the B_R and diminishing the overall heat transfer coefficient by 48.7%. In contrast, symmetric designs like semicircular (B_{SEM}) and polygonal (B_{POL}) performed poorly because of unobstructed heat conduction pathways. Ultimately, this study illustrates that passive geometric optimisation of interior cavities is a more effective approach to improving the thermal resilience of building envelopes in harsh climates.

1. Introduction

Building energy consumption for maintaining indoor living environments has consistently risen, especially amid the ongoing growth of human society. Nowadays, building fields consume 30% of the total energy generated and account for 26% of global energy emissions [1] In hot climate countries, for example, in Iraq, 48% of the generated energy is consumed by buildings, and fifty percent of the amount is spent on adequate indoor living environments [2]. Therefore, developing energy-efficient construction materials and innovative technologies becomes crucial to reducing the total energy consumption of the building's fields. External walls, as one of the essential building components, play a fundamental role in governing heat transfer and, consequently, energy consumption.

Constructive bricks, particularly concrete bricks, are usually employed for their reliable mechanical properties and low cost. Nevertheless, the utilisation of standard concrete masonry structures in hyper-arid regions is restricted by their relatively low thermal resistance. Therefore, it is essential to maintain the mechanical characteristics of masonry units while enhancing their thermal properties. In recent years, various processes have been utilised to improve the thermal performance of bricks by including insulators [3,4], waste materials [5–7], phase change materials (PCM) [7,8] and nanomaterials [9–11]. For example, Seddik Hassan et al. [12]. studied the possibility of improving the bricks' thermal performance by using sludge and sugarcane bagasse ash. The result of the study showed that the thermal conductivity of brick samples created by combining clay, sludge, and sugarcane bagasse ash improved (0.11 to 0.26 W/m·K) relative to conventional brick types (0.33–1.6 W/m·K). Additionally, a 16.5% energy consumption reduction was achieved by the proposed brick walls compared to conventional clay bricks, while enhancing thermal comfort conditions by 6.3%. Moreover, Mahapatra et al. [13] utilised rice husk as a replacement for sand in cement mortar. Their findings showed that the thermal conductivity was decreased by 12% by replacing 7% of sand with rice husk. While significantly enhancing the thermal performance of the bricks, the

* Corresponding author.
E-mail addresses: hayderallami@uomisan.edu.iq (H. Al-lami), hussainbahadly8@uomisan.edu.iq (H. Madhi), diaa.sabeeh@uomisan.edu.iq (D.S.J. Al-Saedi), ali_abbas@uomisan.edu.iq (A.A.H. AlMaidi), eng.mushtaq@uomisan.edu.iq (M.A. Al-Furaiji).

https://doi.org/10.1016/j.rineng.2026.112198
Received 8 June 2026; Received in revised form 12 July 2026; Accepted 24 July 2026
Available online 25 July 2026

Nomenclature

Abbreviations

B_R	Brick without cavities reference brick
B_{CRS}	Brick with cross-shaped cavities
B_{POL}	Brick with polygonal cavities
B_{DIA}	Brick with diamond-shaped cavities
B_{HEX}	Brick with hexagonal cavities
B_{SEM}	Brick with semicircular cavities
B_{TRP}	Brick with trapezoidal cavities
B_{SF}	Brick with shark fin-shaped cavities
B_{TP}	Brick with tilted parallelogram-shaped cavities
CFD	Computational Fluid Dynamics
PCM	Phase change material

Symbol

ρ	Density [kg/m^3]
q_{in}	Internal heat flux
V	Velocity vector [m/s]
P	Static pressure [Pa]
μ	Dynamic Viscosity [kg/m·s]
g	Gravitational acceleration [m/s^2]
β	Thermal expansion coefficient [K^{-1}]
T	Local Temperature [K]
T_{ref}	Reference Temperature [K]
C_p	Specific Heat [J/kg·K]
k	Thermal Conductivity [W/m·K]
S_h	Volumetric heat source term [W/m^3]
I	Radiation intensity [W/m^2·sr]
a	Absorption coefficient [m^{-1}]
σs	Scattering coefficient [m^{-1}]
n	Refractive index
σ	Stefan-Boltzmann constant [W/m^2·K^4]
ϕ	Phase function
Ω'	Solid angle
R	Equivalent thermal resistance [m^2·K/W]
U	Overall heat transfer coefficient [W/m^2·K]
$T_{sol-air}$	Sol-Air Temperature [K]
T_{amb}	Ambient temperature [K]
T_i	Inner temperature [K]
To	Outer temperature [K]
h_{in}	Inner heat coefficient [W/m^2·K]
h_{out}	Outer heat coefficient [W/m^2·K]

mechanical compressive strength has decreased. Kantasiri et al. [14] investigated the incorporation of leftover crumb rubber in concrete bricks for thermal insulation purposes. The research revealed a substantial enhancement in the material's thermal conductivity, rising from 0.51 to 0.67 W/m·K. Consequently, it may serve as a viable option for energy-efficient structures. Nagapan et al. [15] investigated the thermal and mechanical enhancements of including spent mushroom substrate as potential fine aggregates in cement bricks at a ratio of 5% to 25%. The research indicated that augmenting the percentage of spent mushroom substrate could enhance the thermal insulation capabilities of bricks, while decreasing their mechanical characteristics. The thermal conductivity of modified bricks can be reduced by 41.6% to 84.9% in comparison to conventional cement bricks. The mechanical performance investigation revealed that modified bricks with 15% spent mushroom substrate are suitable for non-load-bearing wall partitions, whilst those with 5% can satisfy the compressive strength requirements for load-bearing walls. The incorporation of PCMs into bricks and masonry units has been extensively investigated to enhance thermal storage capacity and energy efficiency in buildings [16,17]. Many researchers have investigated diverse approaches for PCM integration, revealing significant improvements in thermal storage capability, more effective indoor temperature regulation, and appreciable reductions in overall energy consumption. Salman et al. [18] evaluated the thermal and economic performance of incorporating PCMs into building bricks as a strategy to reduce cooling demand and emissions. The study employed numerical simulations using ANSYS Fluent to analyse different brick configurations integrated with RT37, RT42, and composite PCMs. The results indicated that RT37 achieved the best thermal performance, with a maximum temperature reduction of 6.681 °C and a notable decrease in heat gain. The composite PCM provided a balance between thermal efficiency and economic benefits, whereas RT42 showed limited thermal improvement. Additionally, the study reported a reduction in CO_2 emissions of up to 0.11202 kg/day and cost savings of 6.702 IQD/day, confirming the potential of PCM-enhanced bricks as an effective solution for enhancing building energy efficiency and sustainability. Zhang et al. [19]investigated the incorporation of PCMs alongside thermal insulation within concrete masonry unit walls. The research assessed various wall configurations and PCM distributions under different thermal conditions. The findings indicated that the inclusion of PCM significantly increased the thermal inertia of the wall, mitigated thermal bridging, and enhanced both steady-state and transient thermal behaviour. Mukram & Daniel [20]created a distinctive cement brick incorporating micro-encapsulated phase change materials for constructing walls. Their findings demonstrated that altering PCM positioning within the brick has a considerable impact on the decrease in heat flow. The ideal arrangement reduced heat gain by 32% and decreased interior temperatures by 1.2 °C, demonstrating PCM's efficiency for passive cooling applications. Al-Yasiri & Szabó [21] experimentally assessed the thermal performance of concrete bricks containing macro-encapsulated phase change materials, utilising circular, square, and rectangular capsule cross-sections. Seven bricks were evaluated against the reference brick without PCM, utilising a PCM with a melting temperature of around 44 °C. Optimal thermal performance was attained using square-section capsules, resulting in an average maximum internal surface temperature reduction of 1.88 °C, a decrement factor of 0.901, and a time lag of 42.5 min. Several studies have explored the development of masonry units through the incorporation of cavities with diverse geometrical configurations, reporting promising and reasonably consistent enhancements in their overall performance.

Researchers have extensively investigated diverse passive cooling and thermal management strategies in a variety of engineering applications to mitigate severe thermal loads and reduce energy demands in high-temperature environments. In fact, the fundamental principles of computational fluid dynamics (CFD) and geometric flow optimisation are becoming increasingly important in a variety of energy sectors, as they are responsible for performance improvements in a wide range of applications, including the thermal regulation of building envelopes and wind energy harvesting systems [22–24] . A highly efficient method of passive heat mitigation involves optimising geometry to manipulate thermal paths and fluid behaviour. For example, the strategic integration and geometric arrangement of heat-transfer-inducing structures, such as fins or internal baffles, have been shown to significantly alter fluid flow paths and augment or suppress localised heat transfer, depending on the desired thermal outcome [25–33] Moreover, the critical significance of regulating fluid-solid thermal interactions in arid regions, where extreme solar intensities are prevalent, is emphasised by advanced numerical and experimental evaluations of thermal management systems [34–37]. By employing these fundamental principles of fluid-thermal control and geometric optimisation in building envelopes, a promising, zero-cost approach to improving the thermal resistance of masonry structures is provided, without the need for specialised materials.

Aligned with that approach, numerous studies have investigated the creation of masonry units by integrating cavities with various geometric designs, yielding encouraging and essentially constant improvements in their overall performance. Gondim et al. [38] examined the influence of clay hollow block geometry on thermal performance and building energy efficiency using numerical simulations. The study utilised Abaqus/CAE to evaluate the thermal resistance of conventional and modified block designs with similar void ratios, followed by energy analysis using EnergyPlus. The results indicated that optimised internal cavity geometries could reduce thermal transmittance by >30% at the block level and around 20% at the wall level. In terms of energy performance, the improvements were limited during hot periods, while significant energy savings of up to 34% were achieved during colder conditions, highlighting the influence of climate on the effectiveness of geometric modifications. Vera et al. [39] evaluated the thermal performance of hollow clay masonry walls with the aim of reducing the U-value and minimising energy losses. A three-dimensional finite element method was employed to model heat transfer through bricks and walls, with validation based on experimental measurements. The findings indicated that using smaller rectangular hollows can reduce the U-value to 0.761 $W/m^2 \cdot K$, while increasing brick thickness further decreases it to 0.563 $W/m^2 \cdot K$. In contrast, reducing the thermal conductivity of clay showed a negligible effect on the overall wall U-value. Chen et al. [40] analysed the thermal performance of traditional Chinese cavity walls with irregular geometries formed by different bond patterns using a combination of experimental validation and 3D numerical modelling. The results showed that radiation is the dominant heat transfer mechanism within cavities, accounting for approximately 60%, while convection has a minor contribution. The thermal resistance of 240 mm cavity walls ranged between 0.30–0.43 $W/m^2 \cdot K$, with the Flemish bond exhibiting the lowest performance. Additionally, increasing cavity size and wall thickness improved thermal resistance, and cavity walls slightly outperformed solid walls. Brick thermal conductivity and surface emissivity were identified as the most influential parameters, while clay infill proved effective in enhancing thermal performance.

A critical examination of the existing literature reveals that most previous studies have primarily focused on improving the thermal insulation performance of masonry units through material modification, the incorporation of low-thermal-conductivity materials, or insulation enhancement. Although these approaches have demonstrated promising improvements, they are often associated with increased manufacturing complexity and additional costs. In contrast, relatively few studies have systematically investigated the influence of internal cavity geometry on the thermal performance of hollow concrete bricks, and those available generally considered only a limited number of cavity configurations without isolating the effect of cavity geometry from other design parameters. Consequently, the independent influence of cavity geometry under identical geometric, material, and operating conditions remains insufficiently understood. To address this research gap, the present novel study numerically compares eight different symmetric and asymmetric cavity configurations together with a solid reference brick while maintaining identical external dimensions, material properties, and a constant void ratio of 13%. This approach enables a direct assessment of the influence of cavity geometry on the thermal performance of concrete bricks under the severe climatic conditions of Amarah, Iraq. The findings provide new insight into the role of cavity arrangement in enhancing the thermal resistance of hollow concrete bricks and offer practical design guidance for developing energy-efficient masonry units for hot-arid regions. In order to conform to international building codes and architectural engineering standards, this study focuses on dimensional metrics like U-value and R-value. However, it is recognised that dimensionless analysis, such as using Rayleigh and Nusselt numbers, can achieve a broader theoretical generalisation of these conjugate heat transfer (CHT) mechanisms, which is in line with previous fundamental CHT studies [41,42].

2. Methodology

The thermal performance of different hollow concrete masonry units, all with a consistent 13% void ratio but varying internal cavity geometry, was examined using Computational Fluid Dynamics (CFD) through ANSYS Fluent. This study replaces conventional solid-brick analysis with a comparative thermal assessment of eight unique interior structures, including hexagonal, shark-fin, and semicircle forms. The simulations were run under steady-state conditions to evaluate the spatial distribution of temperatures and the heat flux across heterogeneous brick profiles.

The design of each interior cavity aimed to enhance the unit's thermal resistance by interrupting heat-flow pathways and regulating the interplay between solid conduction and internal fluid convection. This study seeks to determine the ideal geometric design for reducing heat input in building envelopes, particularly by replicating the intense solar radiation and ambient temperature conditions characteristic of the arid region of Amarah, Iraq.

Unlike prior studies, which varied the overall air content within a brick, this one maintained a constant 13% void ratio. The 13% limit was chosen to maintain the brick's structural integrity while maximising its heat resistance. By maintaining a constant volume, the study can precisely isolate the effects of various cavity geometries on the interplay between natural air circulation and surface-to-surface radiation. The flowchart in Fig. 1 depicts the procedural framework for this numerical analysis.

2.1. Model's geometry

This study examined the thermal performance of nine different concrete bricks using three-dimensional numerical simulations. An accurate assessment of the thermal efficiency of these models was conducted using ANSYS Fluent after they were developed in SolidWorks. A conventional solid brick (B_R) with exterior dimensions of 0.23 m × 0.12 m × 0.07 m was employed as the baseline control model. Eight different configurations with various interior cavity architectures were created to improve the thermal resistance of the building envelope. Table 1 shows the thermophysical properties of the utilised concrete brick.

As explained in Table 2, which shows the geometrical parameters of the cavities used in the simulation. A very cautious void ratio of 13% was set as a fixed control variable for all hollow models to separate the impact of cavity architecture from that of total air volume. While commercial masonry units often optimise internal air volume to the maximum permits of roughly 50% allowed by the ASTM C90 structural thickness criteria [43], there are two important scientific reasons to maintain a void ratio of 13%. First, it ensures that the masonry units maintain the mechanical integrity necessary for load-bearing walls without requiring further compressive testing by preserving the overwhelming structural mass. Specifically, a void ratio of 13% is more than sufficient to meet the ASTM C90 standard of a maximum void ratio of 25% for a brick to be officially identified as a load-bearing ‘solid’ unit. Second, keeping the air volume intentionally low guarantees that any thermal attenuation that is seen is solely due to geometric manipulation, notably convective stagnation and thermal tortuosity, rather than the simple addition of an insulating air mass. This threshold also shows that under extreme hyper-arid boundary conditions, even small volumetric changes can result in significant thermal gains if the internal architecture is carefully optimised. Fig. 2 shows the examined geometries, which fall into two principal categories based on their structural symmetry. Firstly, symmetric cavity designs include traditional and geometric shapes with mirror-like symmetry, such as cross (B_{CRS}), polygonal (B_{POL}), diamond (B_{DIA}), and hexagonal (B_{HEX}). The other category is asymmetric cavity architectures, which encompass Semicircular (B_{SEM}),

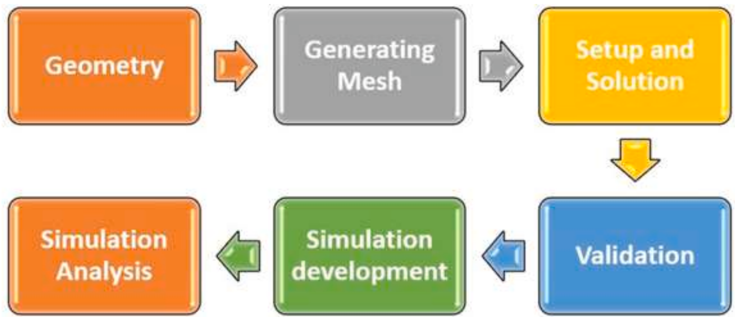

Fig. 1. The procedural framework for the numerical analysis.

Table 1
Thermophysical properties of the utilised concrete brick [44].

Properties	Unit	Concrete brick
Density	kg/m^3	1440
Specific heat capacity	J/kg·K	750
Thermal conductivity	W/m·K	1.4

Table 2
Geometrical parameters of the simulation's employed cavities.

Model name	Quantity	Key Dimensions	Total Void Volume (cm^3)	Void Ratio (%)
B_{CRS}	4	Vertical arm = 3.74 × 1.50 cm, Horizontal arm = 3.74 × 1.50 cm	251.2	13
B_{POL}	4	Regular pentagon, side = 2.28 cm, inscribed radius = 1.57 cm	251.2	13
B_{DIA}	4	Base = 3.56 cm, height = 2.52 cm, tilt angle = 45°	251.2	13
B_{HEX}	4	Side = 1.85 cm	251.2	13
B_{SEM}	4	Radius = 2.39 cm	251.2	13
B_{TRP}	4	Bases = 2.00 cm and 5.18 cm, height = 2.50 cm	251.2	13
B_{SF}	4	Base = 4.48 cm, height = 4.00 cm (one edge is curved)	251.2	13
B_{TP}	4	Base = 4.00 cm, height = 2.24 cm, tilt angle = 30°	251.2	13

Trapezoidal (B_{TRP}), Shark-fin (B_{SF}), and Tilted Parallelogram (B_{TP}).

Rather than using an automated computational optimisation algorithm, the cavity geometries were designed systematically using the physical principles of thermal tortuosity and convective stagnation. The asymmetric architectures, specifically the Tilted Parallelogram (BTP) and Shark-fin (BSF), were intended to disrupt direct, linear conduction paths. As a result, the interior gaps were intentionally placed to reduce the "thermal bridge" effect while preserving the structural integrity necessary for masonry applications, which is important for sustaining energy efficiency and preventing heat loss in buildings.

3. Setup and solution

3.1. Assumption

To minimize computational complexity while preserving high physical accuracy, the numerical model was built using the following assumptions:

1. Steady-State Conditions: The thermal study is carried out in steady-state conditions to determine the peak thermal performance of the brick models.
2. Material Isotropy: The concrete matrix is assumed to be homogeneous and isotropic, having constant thermal characteristics.
3. To simulate buoyancy-driven natural convection, the Boussinesq approximation governs density fluctuations within the internal air cavities.
4. Natural convection within the internal air-filled cavitys is laminar.
5. No-slip and no-penetration boundary conditions were implemented on all solid surfaces.
6. Although the steady-state approach effectively isolates the influence of geometry on peak thermal resistance, it is crucial to acknowledge that actual building envelopes exhibit transient behaviour in response to daily solar fluctuations. As a result, this investigation does not capture thermal mass phenomena, including the decrement factor and time lag. Future 24-hour simulations will concentrate on these dynamic effects.

3.2. Solving governingequations

The steady-state thermal performance and surface temperature response of concrete masonry units were assessed by solving the conjugate heat transfer and internal cavity radiation using the conventional governing transport equations in ANSYS Fluent. In accordance with the numerical simulation framework provided by Svoboda and Kubr [45] for hollow brick, the system maintains the conservation of mass, momentum, and energy, in conjunction with the usual closure equations as detailed below.:

3.2.1. Continuity equation

This equation represents the conservation of mass within the computational domain:

$$\nabla .\left(\rho \vec{V}\right) = 0 \tag{1}$$

3.2.2. Momentum equation

The Boussinesq approximation is employed to model temperature-dependent density fluctuations in buoyancy-driven natural convection within the 13%-void enclosures. To quantitatively explain this approach, the localized temperature changes within the cavities are relatively small ($\Delta T \approx 5 - 15\ K$). At ordinary operating temperatures, with an air thermal expansion coefficient of $\beta \approx 0.0033\ K^{-1}$, the validity parameter $\beta\Delta T$ remains far below the $\beta\Delta T \ll 1$ limit, proving its stringent validity for this investigation.

$$\nabla.\left(\rho \vec{V}\vec{V}\right) = -\nabla P + \nabla\left(\mu\nabla\vec{V}\right) + \rho g\beta\left(T - T_{ref}\right) \tag{2}$$

3.2.3. Energy equation

The energy conservation equation for the coupled solid-fluid domain includes a radiative source term (S_h) to connect the thermal field with the radiation model, natural convection in the fluid, and conduction in the solid concrete matrix. The equation is natively reduced to pure steady-state conduction in the solid concrete domain, as the fluid

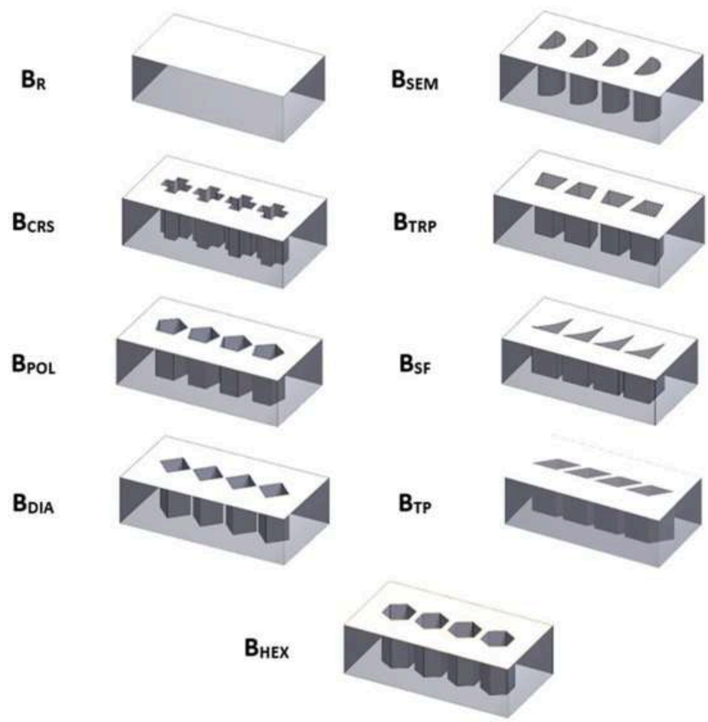

Fig. 2. Model geometries.

velocity vector is zero ($\overrightarrow{V}=0$):

$$\nabla.\left(\rho\overrightarrow{VC_p}T\right) = \nabla\cdot(k\nabla T) + S_h \tag{3}$$

3.2.4. *Radiative transfer equation (Discrete ordinates model)*

The internal heat transfer within the 13% void cavities was calculated using the Discrete Ordinates (DO) radiation model. Although the air was considered a non-participating medium, the DO model was used to capture the surface-to-surface radiative exchange between the internal cavity walls. This guarantees that each shape's overall thermal resistance reflects the combined effects of conduction, natural convection, and radiation. To ensure a conservative and stringent thermal evaluation, the fluid-solid interfaces within the internal cavities were simulated with an emissivity of 1.0, a worst-case black-body approximation that optimises internal radiative heat exchange.

The radiation intensity I at the position r and in the direction, s is defined as [46]

$$\nabla.(I(r,s)s) + (a+\sigma_s)I(r,s) = an^2\frac{\sigma T^4}{\pi} + \frac{\sigma_s}{4\pi}\int_0^{4\pi} I(r,s')\varphi(s.s')d\Omega' \tag{4}$$

Using Eq. (5), it is possible to obtain the thermal transmittance of the brick U [W/m^2 K]:

$$U = \frac{1}{R} \tag{5}$$

Where R is the thermal resistance of the brick [m^2 K/W]

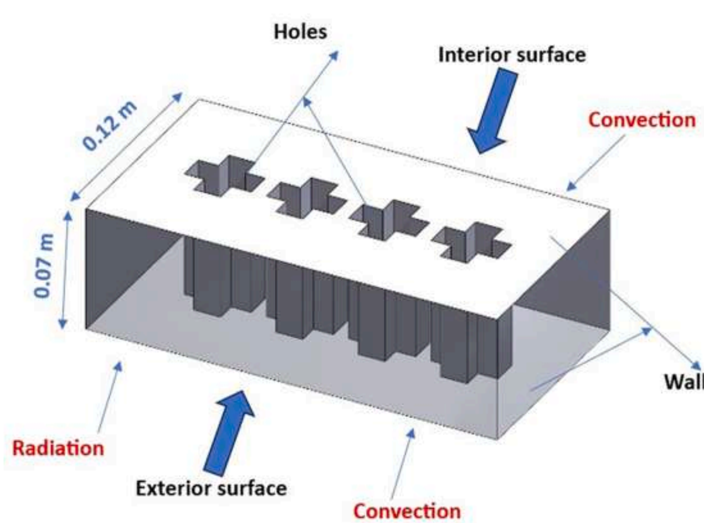

Fig. 3. A three-dimensional schematic representation of the computational domain.

3.3. Boundary conditions

The thermal response of the nine models was assessed by executing the numerical model under steady-state conditions. The boundary conditions were set up in order to accurately depict the extreme summer climate of Amarah, Iraq (Fig. 3). A detailed summary of all employed thermal parameters is shown in Table 3. The specific conditions were implemented as follows:

1- A fixed temperature boundary condition was applied to the brick's outer face. To account for the simultaneous effects of ambient air temperature and incident solar radiation, this temperature, $T_{sol-air}$, was pre-calculated for five scenarios using the ambient temperature $T_{amb}$and solar irradiance G data sourced from [47] for the Amarah region. The computation was done using the usual Sol-Air formula [8]:

$$T_{sol-air} = T_{amb} + \frac{\alpha.G}{h_{out}} \tag{6}$$

Where α is the solar absorptivity of the concrete surface. which was assigned a standard value of 0.65 in accordance with ASHRAE Fundamentals [48].

h_{out} is the outdoor convective heat transfer coefficient, which was adjusted for each scenario to reflect the local environmental conditions, as shown in Table 3.

2- The inside surface of the brick delineates the limit exposed to the indoor living space. To objectively assess the cooling load and heat gain across all 9 geometries, the following conditions were implemented:
- A constant inner temperature (T_i) of 298 K was set. This complies with global requirements for interior thermal comfort in air-conditioned buildings.
- A constant convective heat transfer coefficient h_{in} of 8.29 W/m2. K was employed. This value is the ASHRAE standard for indoor vertical surfaces under "still air" conditions

3- The internal heat transfer in the air-filled cavitys was modelled as a coupled Multiphysics phenomenon. The solver employs a linked technique that simultaneously accounts for thermal interactions between the concrete matrix and internal air volumes, eliminating the need for predetermined interface temperatures. This methodology guarantees accurate resolution of natural convection (induced by buoyancy) and surface-to-surface radiation (simulated using the discrete-ordinates method) across all 8-cavity geometries.

4- The contributions of conduction, natural convection and radiation were not individually quantified, but all were evaluated in a coupled manner for the overall conjugate heat transfer since the principal objective was to obtain the overall thermal resistance and transmittance of the building envelopes.

Table 3
A detailed summary of all employed thermal parameters.

Parameter	Value	unit
T_{in}	298	K
h_{in}	8.29	$W/m^2 \cdot K$
α	0.65	-
h_{out} / $T_{sol-air,\ at\ 7\ AM}$	42/ 310	$W/m^2 \cdot K\ /\ K$
h_{out} /$T_{sol-air,\ at\ 9\ AM}$	160/ 319.9	$W/m^2 \cdot K\ /\ K$
h_{out} /$T_{sol-air,at\ 11\ AM}$	42/ 338.6	$W/m^2 \cdot K\ /\ K$
h_{out} /$T_{sol-air,at\ 1\ PM}$	42/ 341.3	$W/m^2 \cdot K\ /\ K$
h_{out} /$T_{sol-air,at\ 3\ PM}$	20/ 342.5	$W/m^2 \cdot K\ /\ K$
h_{out} /$T_{sol-air,at\ 5\ PM}$	2/337.3	$W/m^2 \cdot K\ /\ K$

3.4. Numerical setup

The mathematical model established by the governing equations was resolved utilising the Finite Volume Method in the ANSYS Fluent 19.1 environment. To guarantee the precision and consistency of the steady-state thermal analysis over all 9 different cavity geometries, the following numerical setups were employed:

1. The coupled algorithm was employed for pressure-velocity coupling. In contrast to segregated solvers, this method simultaneously solves the momentum and continuity equations, thereby enhancing stability for buoyancy-driven flows in air cavities.
2. High-order accuracy was preserved across an entire domain. A Second-Order scheme was employed for pressure, whilst a Second-Order Upwind scheme was utilised for momentum, energy, and the discrete ordinates (DO) radiation model. This reduces numerical diffusion and guarantees accurate heat gradients around the cavity geometries.
3. A rigorous convergence method was implemented. The absolute residuals for continuity, velocity and energy were kept below 10^{-6}.

3.5. Mesh generation and grid-independent test

To confirm the numerical accuracy of the simulations across all selected cavity geometries, a grid independence study was conducted. The mesh was refined throughout seven layers, with the element count growing from 1932 to 9120. The inner temperature and heat flux were used as major indicators of solution convergence.

As demonstrated by Figs. 4 and 5, the solution became essentially independent of grid density until the element count reached roughly 5610 (equivalent to a 0.007 m element size). At this level, the difference in inner temperature was <0.01 K when compared to the next, and the heat flux demonstrated a negligible relative error of <0.05%. In addition, to fully quantify this stabilisation, the relative percentage errors for both parameters between successive grids were determined and summarised in Table 4.

Further refining to 9120 elements resulted in no significant improvement in thermal accuracy while significantly increasing computational cost. Consequently, the mesh size of 0.007 m (5610 elements) was used for all further simulations. This choice strikes the ideal mix between computational economy and solution fidelity, guaranteeing that the thermal gradients surrounding the 13% void structures are fully resolved. This technique is consistent with existing CFD best practices [49,50], which states that a stable solution with little relative error is adequate to ensure mesh independence.

3.6. Validation against experimentalmeasurements

To verify the accuracy and reliability of the developed numerical framework, the present CFD model was validated against the experimental data reported by Al-Yasiri and Szabó [47], who experimentally investigated the thermal performance of concrete bricks under the harsh summer climatic conditions of Amarah, Iraq. The reference study examined three concrete brick configurations, namely a conventional concrete brick, a brick incorporating PCM capsules, and a brick containing a PCM layer. The experiments were conducted under real outdoor exposure, where the brick specimens were subjected to the prevailing climatic conditions of Amarah, and their thermal response was monitored throughout the daily thermal cycle.

The validation was performed by comparing the predicted and experimentally measured outer and inner surface temperature profiles under representative thermal boundary conditions consistent with those reported in the reference study. As illustrated in Figs. 6 and 7, the numerical model accurately reproduced the measured thermal behaviour, demonstrating excellent agreement between the predicted and experimental temperature distributions throughout the testing period. The

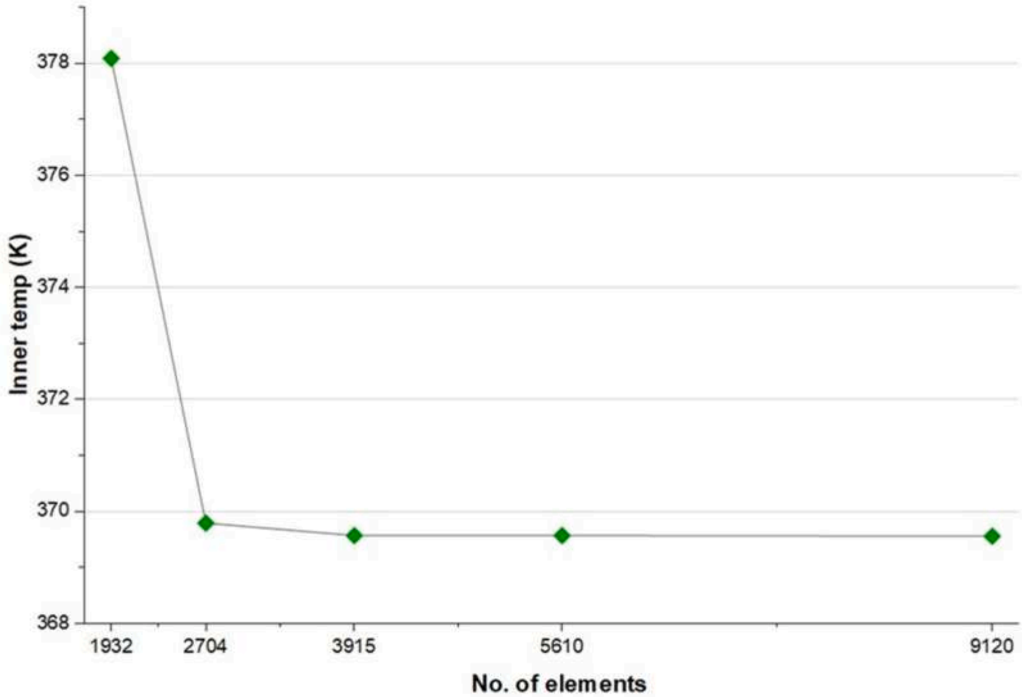

Fig. 4. Influence of the mesh number on the calculated inner temperature for the brick.

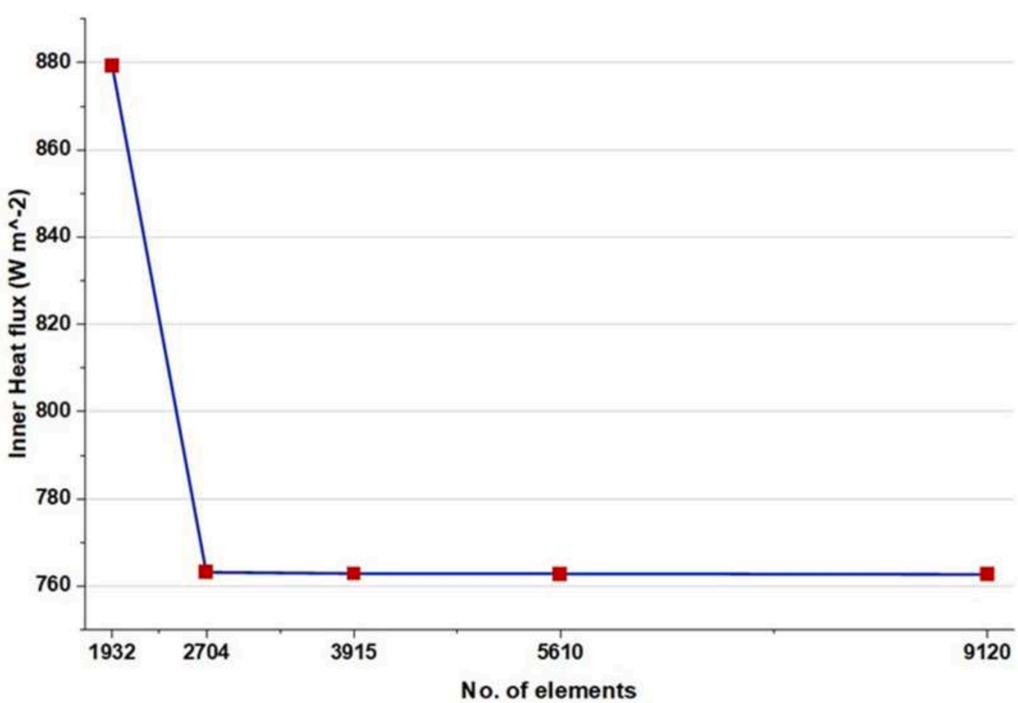

Fig. 5. Influence of the mesh number on the calculated inner heat flux for the brick.

maximum relative deviation between the numerical predictions and the experimental measurements was found to be 2.4%. Additionally, the inner and outer surface temperatures exhibited notably low average deviations, with values of 0.30% and 0.29%, respectively. These tiny differences are due to unavoidable experimental uncertainties, including fluctuations in ambient weather conditions and the measurement accuracy of the thermocouples.

The close agreement between the numerical and experimental results confirms the robustness and predictive capability of the developed CFD model for simulating heat transfer through concrete bricks under severe climatic conditions. Consequently, the validated numerical framework was employed with confidence to evaluate and compare the thermal performance of the proposed cavity configurations under identical operating conditions.

Table 4
Mesh independence study with computed relative errors.

Mesh Elements	inner temp [K]	Relative error %	heat flux [W m^−2]	Relative error %
1932	378.09	-	879.30	-
2704	369.59	2.247	763.22	13.201
3915	369.57	0.01	762.92	0.040
5610	369.57	<0.01	762.90	0.002
9120	369.57	<0.01	762.75	0.020

4. Results and discussion

4.1. Thermal contouranalysis

The qualitative assessment of the thermal performance of different-cavityd bricks is performed by analysing temperature contours recorded during the peak thermal intensity at 1:00 PM. The contours depicted in Figs. 8, 9, and 10 visually represent the depth of heat penetration and the temperature gradients within the solid concrete matrix and the internal air cavities. By analysing the distribution of thermal fields, the influence of each shape on the interruption of conductive heat transfer becomes distinctly recognisable.

The thermal contours in the Reference Brick (B_R), appear as uniform, parallel bands moving from the exterior to the internal surface. This linear distribution indicates continuous conduction paths where heat travels along the path of least resistance, resulting in significant thermal bridging that causes increased internal surface temperatures. Nevertheless, the incorporation of hollow cavities, in particular the B_{TP} and B_{HEX} configurations, substantially alters these isotherms. The air stagnation within the enclosed cavities functions as a high-resistance barrier, causing heat to detour around the cavities and resulting in a "bottleneck" effect that substantially lengthens the conduction paths. This behaviour illustrates that the geometric configuration efficiently redirects thermal flux, inhibiting deep heat penetration into the interior surface.

The B_{TP} design contours distinctly indicate a significant concentration of elevated temperatures (red and orange areas) at the outside periphery of the brick, but the core and inner portions are maintained within the lower temperature spectrum (green and blue areas). This results directly from the stagnant air in the triangular cavities functioning as a heat insulator. The stagnant air offers significant temperature resistance, effectively "shielding" the inside surface. Conversely,

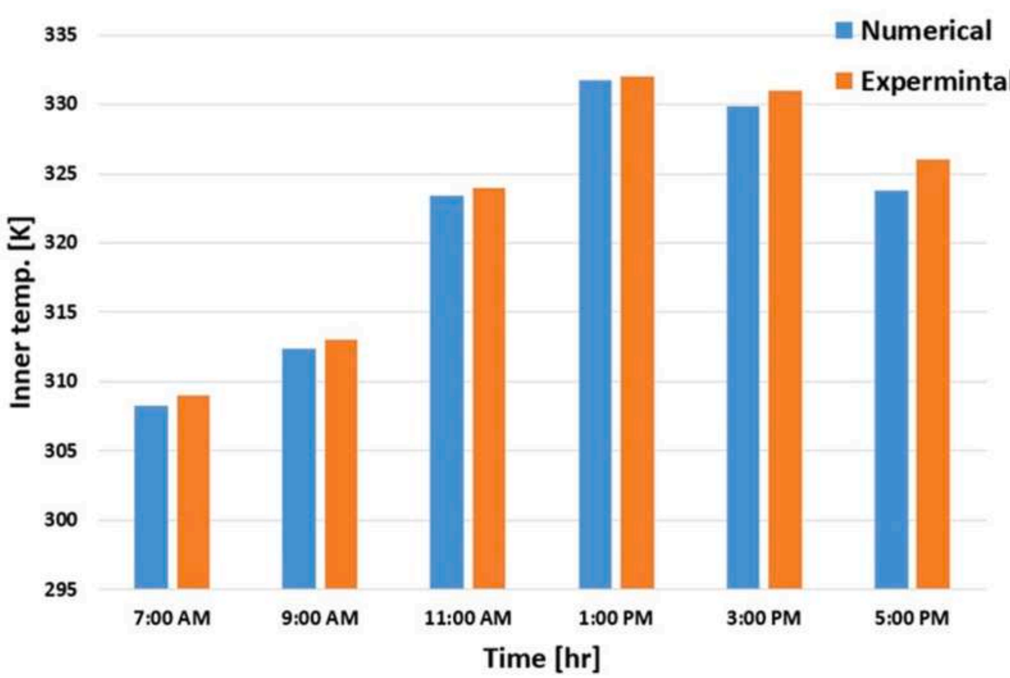

Fig. 6. Validation of numerical results of inner temperature with the experimental study [47].

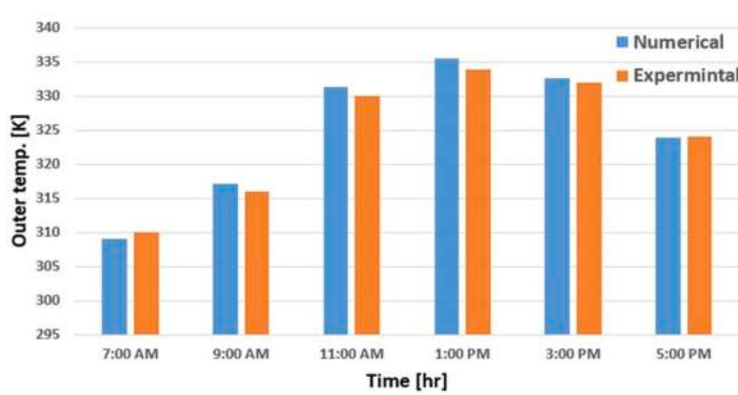

Fig. 7. Validation of numerical results of outer temperature with the experimental study [47].

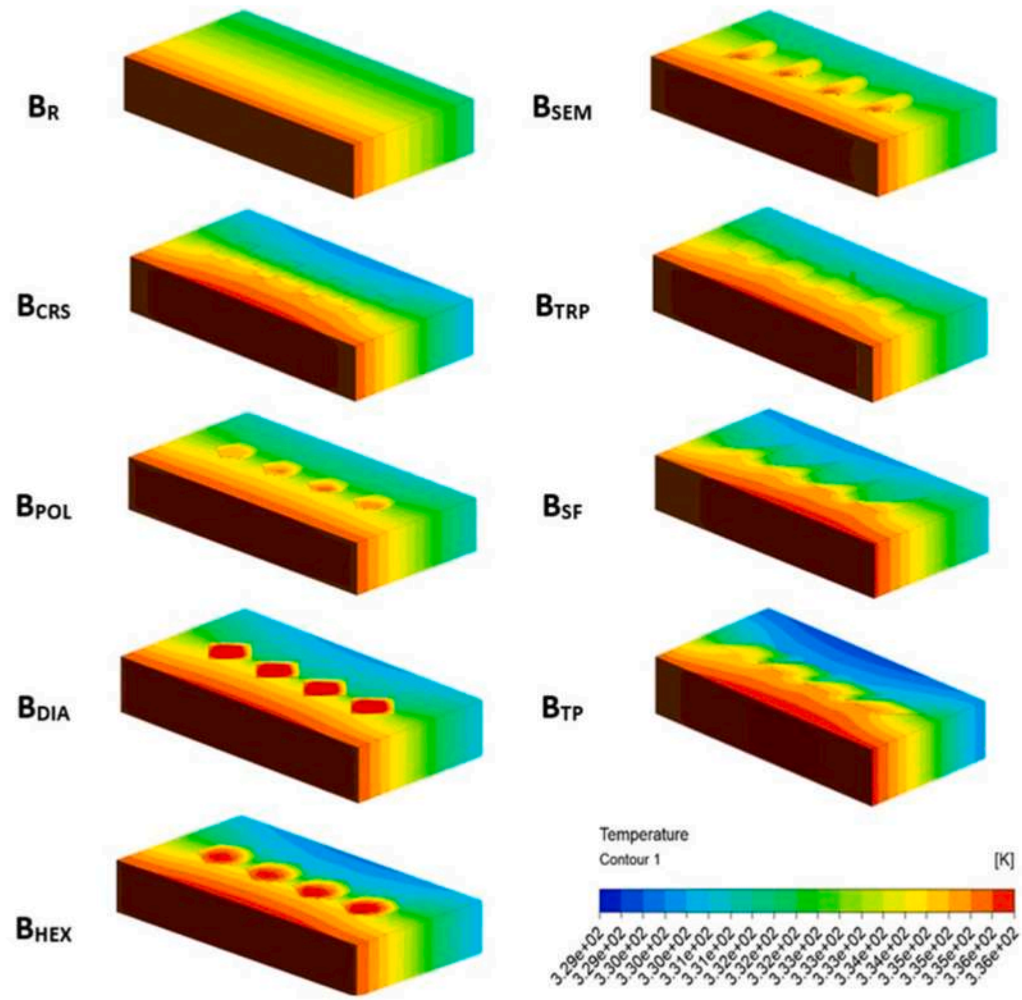

Fig. 8. An isometric view of the temperature contour of the nine models.

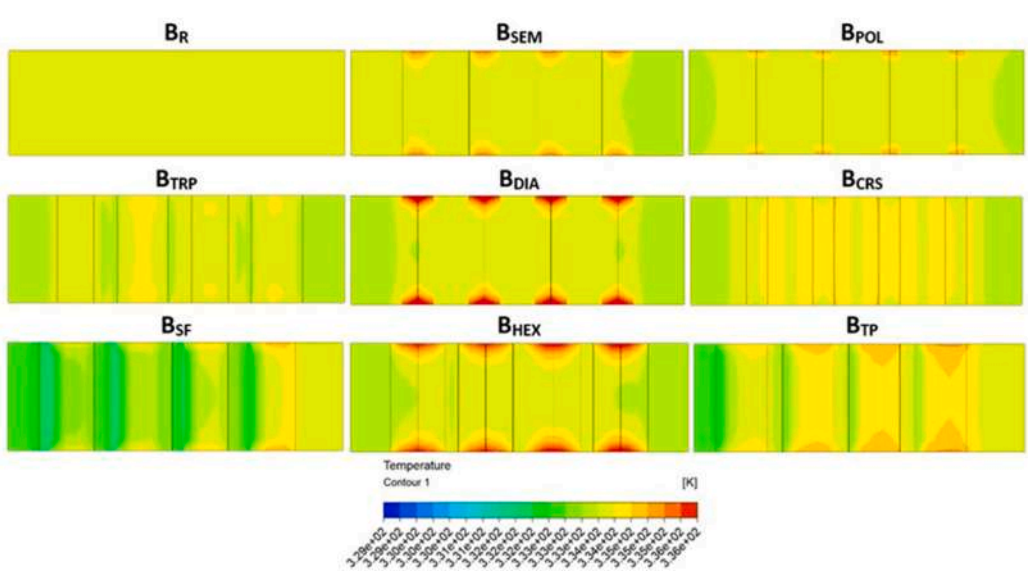

Fig. 9. Temperature distributions of studied geometries at the mid-plane at z = 5 cm.

simpler geometries such as the B_{POL} and B_{SEM} bricks exhibit significantly wider conduits for heat conduction, forming direct thermal bridges that allow thermal fields to permeate more readily through the substantial vertical concrete portions.

Consequently, the thermal contour analysis verifies that the B_{TP} design offers the most efficient thermal barrier. This structure optimises

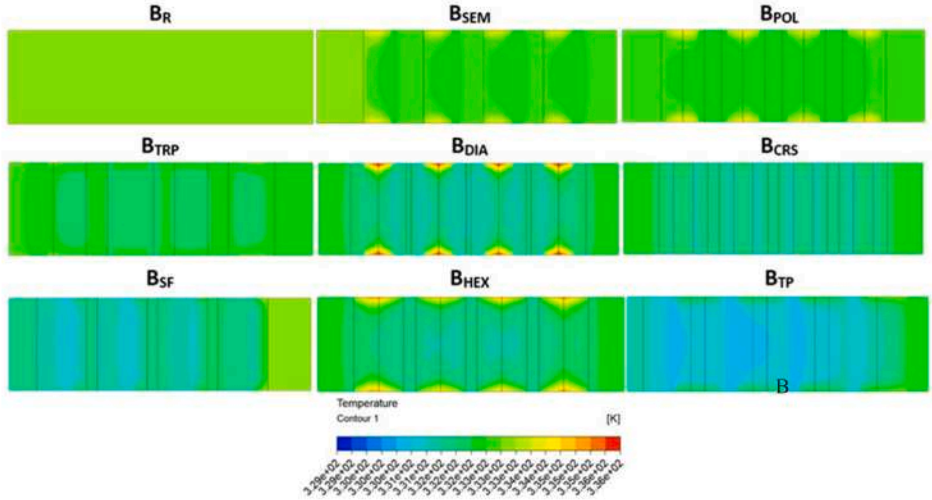

Fig. 10. Temperature distributions of studied geometries at the mid-plane at z = 7 cm.

thermal gradient disruption and restricts peak temperatures to the outer layers, ensuring superior interior thermal comfort. This qualitative data immediately supports the quantitative decreases in heat flow and internal surface temperatures detailed in the next sections, thus strengthening the choice of the B_{TP} design as the superior approach for building insulation in the hot climate of Amarah.

4.2. Analysis of surfacetemperaturegradients

The thermal performance of the proposed brick units is primarily assessed by the interaction between external environmental loads and the resultant internal thermal response. Fig. 11 depicts the fluctuation of the outside surface temperature for the nine models throughout a standard daylight cycle (7:00 AM to 5:00 PM) under the severe heat circumstances of Amarah, Iraq. This investigation is essential for understanding the interaction between solar radiation and ambient temperature with the brick's exterior before heat transfer through the different internal hollow shapes.

The figure illustrates a distinct daily thermal cycle aligned with rising solar intensity. The outer surface temperatures start at roughly 309 K at 7:00 AM. As sun irradiance escalates towards midday, temperatures consistently increase, attaining a maximum of around 336 K at 1:00 PM. This pattern demonstrates the effective implementation of the $T_{sol-air}$ boundary condition, which incorporates both ambient temperature and incident solar radiation. Significantly, there is a negligible variance in outer temperature T_o among the analysed cases, encompassing the baseline Reference Brick (B_R), symmetric configurations (B_{CRS}, B_{POL}, B_{DIA}, B_{HEX}), and asymmetric configurations (B_{SEM}, B_{TRP}, B_{SF}, B_{TP}). This consistency verifies that the exterior thermal input remained constant across all simulations, guaranteeing that any future differences in internal performance are exclusively due to the internal cavity layouts rather than variable boundary circumstances.

Whereas the external thermal loads remain stable, Fig. 12. illustrates that the inner surface temperatures $T_{i,}$ display significant fluctuations depending on the configuration of the internal cavities. Despite all models starting the cycle at a stabilised temperature of roughly 308 K at 7:00 AM, the rate of temperature increase at the inner face is markedly slower than that of the exterior, indicative of the thermal lag and resistance afforded by the concrete matrix and the 13% air-filled cavities. The B_R regularly exhibits the greatest T_i, reaching around 331 K at

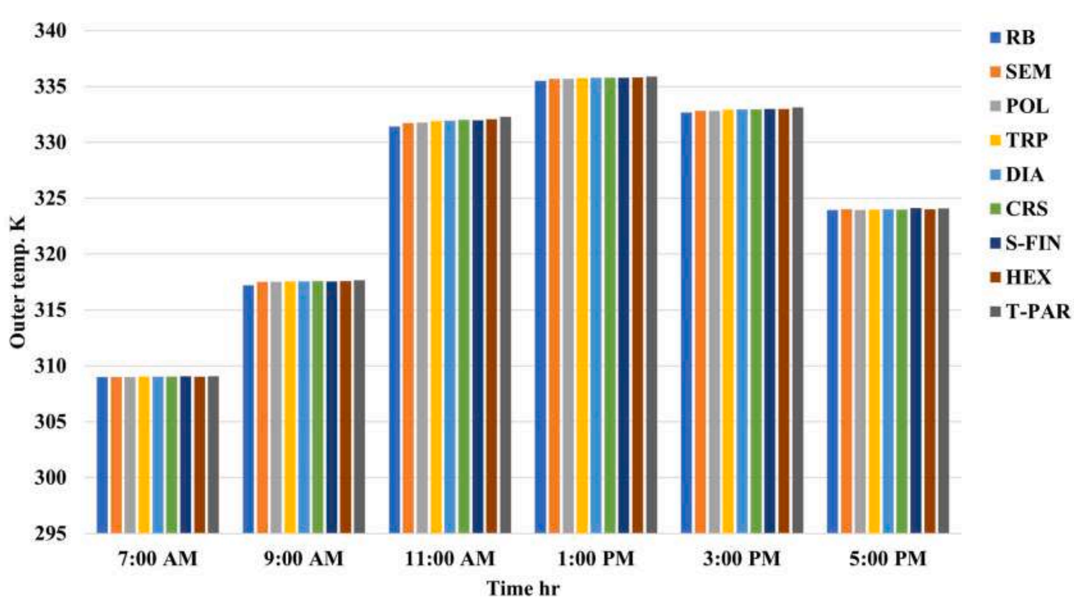

Fig. 11. Variation of Bricks' outer temperature with time during the day for all nine cases.

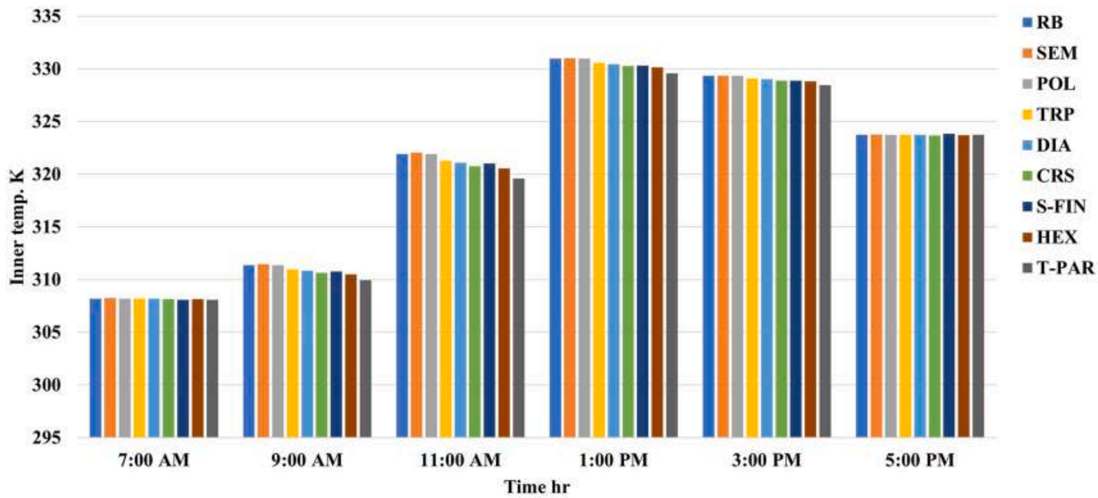

Fig. 12. Variation of Bricks' Inner temperature with time during the day for all nine cases.

1:00 PM, confirming the restricted insulating efficacy of solid concrete in arid regions.

The modified brick models, on the other hand, show different levels of efficacy in stopping heat transfer. Both models, B_{TP} and B_{HEX}, are identified as the most efficient designs, maintaining the lowest internal surface temperatures throughout peak hours. The B_{HEX} model exhibited a notable boost compared to the baseline Reference Brick, attaining a temperature reduction of 11.51 K, equating to a 43.76% improvement in thermal shielding effectiveness. Nevertheless, the B_{TP} proved to be the most efficient configuration, yielding a temperature reduction of 12.68 K a 58.44% improvement compared to the B_R. The B_{HEX} design efficiently employs air chambers to mitigate heat, whereas the B_{TP} asymmetric and inclined configuration is superior at reducing localised thermal bridges. It exhibited an inner surface temperature approximately 1.0 K lower than the B_{HEX} design (319.60 K compared to 320.56 K), hence reinforcing its designation as the superior configuration for extreme arid climates.

The discrepancy between a uniform T_o and a fluctuating T_i indicates that the enhancements in thermal performance are exclusively attributable to geometric optimisation. By sustaining a reduced temperature at the internal border, models such as B_{TP} substantially diminish the total heat flux entering the indoor environment, thereby lowering the energy demand for air conditioning. The thermal resistance is important during peak solar intensity from 11:00 AM to 3:00 PM, designating the B_{TP} arrangement as the most effective for improving thermal comfort in the Iraqi climate.

4.3. Total heatfluxreduction

The internal heat flux (q_{in}) denotes the instantaneous energy transfer rate through the brick and is a vital measure of the building envelope's energy savings potential. Fig. 13 illustrates that all hollow shapes exhibit a significant decrease in heat flux relative to B_R. The reduction is mainly due to the incorporation of air-filled cavities. The extent of this attenuation varies considerably between geometries, demonstrating that the spatial configuration of the 13% void ratio is the primary determinant in thermal regulation.

The B_{TP} geometry proved to be the most efficient design, achieving a maximum heat-flux reduction of about 18% at 11:00 AM (decreasing the load from 244.4 W/m^2 to 200.6 W/m^2). This exceptional performance is basically based on the principle of thermal tortuosity. The B_{TP} design efficiently eradicates direct, quasi-linear conductive pathways and disrupts direct radiative view factors by the use of a staggered and slanted triangle configuration. In a conventional solid brick, heat travels a direct 12-cm channel, while in the B_{TP} design, conductive heat is compelled to follow a considerably extended and complex route around the cavities.

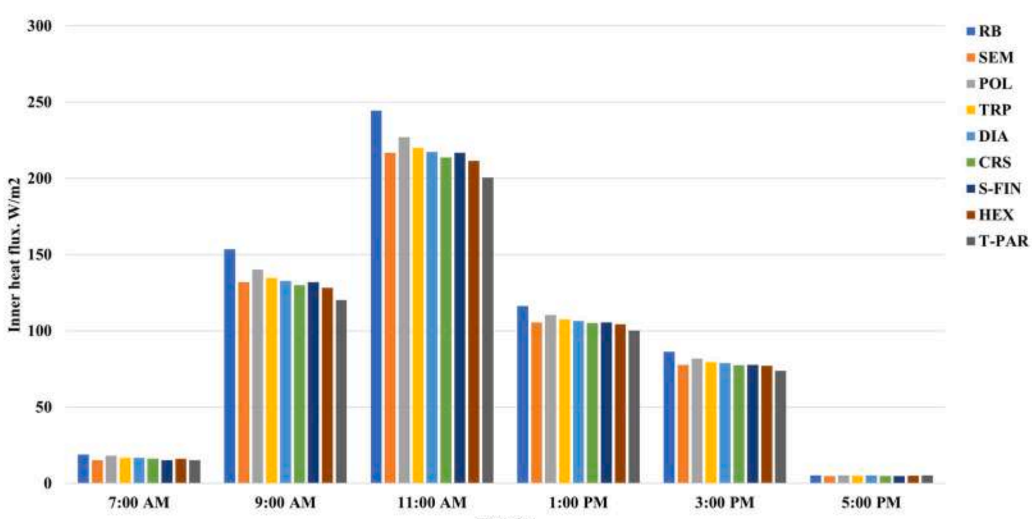

Fig. 13. A comparison of the Inner Surface Heat Flux for all nine models.

This path extension enhances the unit's thermal resistance without necessitating extra material mass or thickness.

A secondary level of performance is noted in the (B_{HEX}) and (B_{SF}) configurations. The B_{HEX} design employs angled internal walls to disrupt the continuity of solid concrete bridges, resulting in a flux reduction of around 13.1%. Likewise, the B_{SF} structure demonstrates superiority by functioning as a series of internal baffles. These fins inhibit natural convection within the air cavities by limiting the development of extensive, high-velocity air recirculation loops and internal circulation cells. The B_{SF} design maintains a relatively stationary internal air environment, ensuring that heat transfer is mostly governed by the slow mechanism of air conduction rather than by faster convective currents.

Conversely, symmetric and simpler geometries, including the B_{DIA}, B_{CRS}, and B_{TRP} models, demonstrated moderate efficacy. Furthermore, B_{POL} and B_{SEM} designs exhibited the lowest performance among the hollow models, remaining nearest to the B_R baseline **due to their higher effective shape factors and unobstructed conductive pathways**. These findings highlight a crucial conclusion for masonry design: the geometric orientation and the capacity to interrupt thermal bridges are significantly more important for energy efficiency than the simple existence of internal air spaces.

4.4. Equivalent thermalresistance(R-Value) and overallheattransfercoefficient(U-Value)

The steady-state metrics of Equivalent Thermal Resistance (*R*) and Overall heat transfer coefficient (*U*) are employed to quantitatively assess the insulating efficacy of the proposed designs. A standardised framework for evaluating the energy-saving potential of various cavity configurations is provided by the parameters that are obtained from the simulation data. The thermal properties of the construction component are substantially altered by the transition from a solid structure to a hollow form with a 13% void ratio, as demonstrated in Figs. 14 and 15.

From Fig. 14, it can be seen that the B_{TP} design presents the most significant impediment to conductive heat transfer during the diurnal cycle, as evidenced by the R-value findings. The B_{TP} design optimises the utilisation of stagnant air as an insulating medium by directing the temperature gradient to interact with staggered, asymmetric cavities. The B_{TP} model's increased R-value suggests greater thermal attenuation capacity, which is essential for mitigating the effects of the high-amplitude solar radiation characteristic of the Amarah region. Air volume is not the sole factor contributing to the increased resistance; rather, it is the result of a "tortuous" conductive pathway that considerably increases the distance that heat must travel from the exterior to the interior surface.

Moreover, as shown in Fig. 15, the *U*-value analysis demonstrates a substantial reduction in the rate of heat transfer for the improved designs. The B_R brick exhibits a high transmittance rate, indicating a significant cooling load requirement. Nonetheless, the B_{TP} and B_{HEX} designs regularly provide significantly lower *U*-values, even during peak solar periods. This inverse link validates the dependability of the numerical model; as the internal geometry disrupts thermal bridges, the U-value diminishes, signifying a direct drop in potential energy consumption for indoor climate control.

A notable discovery from this comparative investigation is the performance disparity between the B_{TP} and more basic hollow designs, such as the B_{SEM} or B_{POL} models. Despite possessing identical void ratios, the B_{SEM} and B_{POL} models demonstrate higher *U*-values and lower *R*-values compared to the B_{TP}. This discrepancy highlights that vertical or symmetric solid bridges enable relatively efficient "high-conductivity highways," whereas the inclined configuration of the B_{TP} design significantly obstructs these paths. Thus, for high-performance building envelopes in arid climates, the geometric optimisation of interior cavities is as crucial as the choice of masonry materials.

4.5. Practical considerationsfor real-worldinstallation

The transition from numerical optimisation to physical building demands a balance of thermal efficiency, structural integrity, and manufacturability. Although models demonstrate that the advanced internal B_{TP} design exhibits greater thermal performance, the practical success of the normal brick is contingent upon the interior structure's capacity to manage mechanical loads. Structurally, while the sloped interior walls of the BTP design act as diagonal bracing to improve lateral shear stability, the acute internal angles may cause localised stress concentrations under large vertical compression pressures. To avoid micro-cracking, careful attention to structural details is required, such as a slight corner filleting. Moreover, by sustaining a 13% vacancy ratio within the rectangular exterior, the design adheres to contemporary industry benchmarks for material savings.

The acute angles of the BTP cavities pose a challenge for standard dry-mix concrete extrusion from a manufacturing perspective. To ensure that the sharp internal corners are fully compacted without honeycombing or tearing during demolding, it is necessary to use high-precision steel dies and carefully control the flowability of the concrete mix. Nonetheless, the brick stays economical as it utilises the

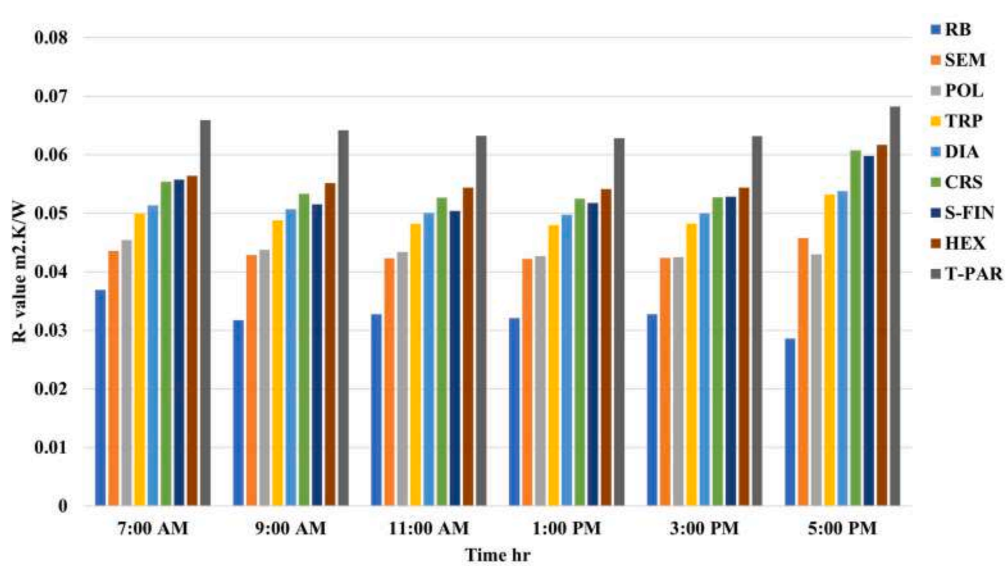

Fig. 14. A comparison of the Thermal Resistance for all nine models.

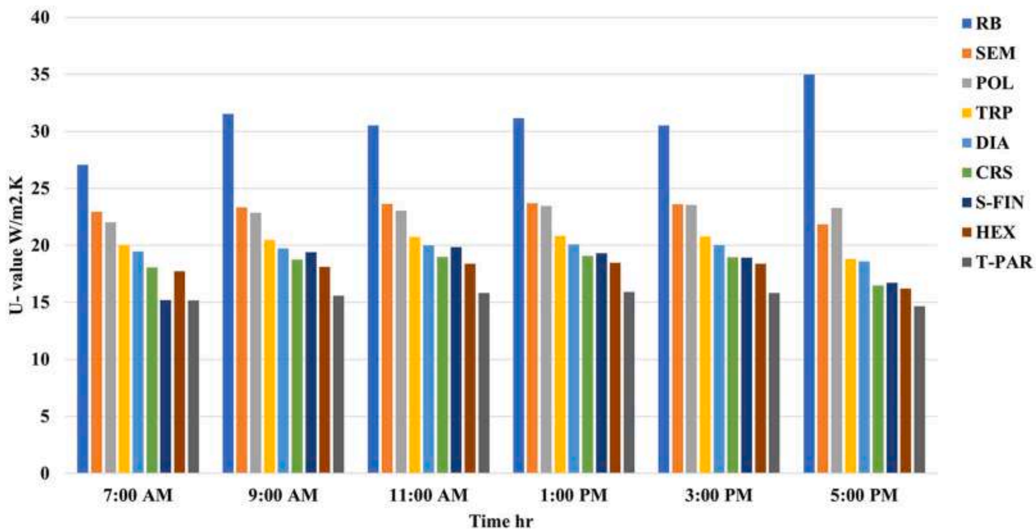

Fig. 15. A comparison of the Overall heat transfer coefficient for all nine models.

stagnant air within its cavities as the principal insulator. By eschewing costly chemical fillers, these bricks offer a cost-effective method to mitigate the thermal load on residential structures in hot areas such as Amarah. The thermal advantages are contingent upon proper installation. The rectangular bricks must be positioned with the interior B_{TP} cavities oriented perpendicular to the thermal flow. This guarantees the complete realisation of the higher thermal resistance identified in the study. The B_{TP} configuration integrates structural integrity with established energy efficiency, presenting a viable, high-performance option for contemporary construction in arid environments.

5. Conclusion

This study performed an original, comprehensive numerical analysis of the thermal efficiency of eight unique internal cavity configurations for concrete bricks, specifically tailored for the harsh climate in Amarah, Iraq. The study identified the geometric design of the internal cavitys as the important variable by sustaining a consistent void ratio of 13%. The findings demonstrate that the internal architecture of a brick is as essential as its material composition for thermal insulation.

The principal quantitative and qualitative findings are as follows:

- The thermal response of the bricks was primarily influenced by the dynamic interaction between the external ambient temperature and solar heat flux. The exterior loads served as the principal factors influencing the temperature gradients at the solid-fluid interface, regulating the maximum heat gain within the interior.
- Among the nine examined designs, the B_{TP} brick was recognised as the optimal solution for thermal mitigation. It enhanced thermal tortuosity by disrupting the symmetry of the internal concrete bridges, efficiently redirecting heat flow and postponing the peak thermal load from reaching the inner face.
- At midday, the B_{TP} brick attained a maximum R-value of 0.063 $m^2 \cdot K/W$, signifying a 96.87% enhancement in thermal resistance relative to the solid Reference Brick (B_R) baseline of 0.032 $m^2 \cdot K/W$. However, this absolute value remains low when compared to contemporary global building envelope insulation standards. This is due to the fact that the present investigation assesses a solitary, independent concrete masonry unit. This unit is intended to serve as the structural basis of a multi-layer wall assembly in practical construction applications. When conventional internal plastering, external rendering, and standard cavity insulation boards are combined, the cumulative thermal resistance of the entire wall envelope will be in compliance with the international energy-efficiency standard.
- The fluid flow analysis verified that the air in the small-scale B_{TP} cavities remains predominantly stationary. The inhibition of natural convection enables the air to serve as an effective insulating layer, forming a high-resistance barrier that markedly diminishes the overall heat flux entering the unit.

In summary, the findings indicate that passive geometric optimisation of interior air cavities, particularly through tilted, staggered layouts, is an excellent method for improving the thermal resilience of building envelopes. The B_{TP} design is endorsed as a technically advanced option for energy-efficient building in arid areas, demonstrating a verified decrease in cooling load without requiring supplementary insulating materials. By successfully integrating the physical mechanisms of thermal tortuosity and convective suppression, this design offers a very practical, zero-cost engineering solution for load-bearing masonry in sustainable urban development.

6. Future work

This study's numerical findings suggest multiple directions for further research to enhance the applicability of the optimised cavity designs.

1. Performing experimental compressive strength and structural load-bearing assessments on the innovative cavity designs, namely the superior Tilted Parallelogram (T-PAR) geometry, to verify adherence to international masonry building standards.
2. Assessing the thermal efficacy of filling the optimised Tilted Parallelogram (T-PAR) cavities with Phase Change Materials (PCMs) to merge geometric insulation with latent heat storage.
3. Simulating brick models under dynamic, 24-hour varying weather conditions to explicitly quantify their dynamic thermal time lag and decrement factor.
4. Exploring more intricate polygonal and curved cavity configurations to develop a more extensive database of shape-dependent thermal resistance.
5. Conducting a thorough sensitivity analysis that explicitly evaluates the trade-offs between thermal performance and structural load-bearing integrity by varying baseline material thermal conductivities and void ratios (e.g., 10% to 20%).
6. Translating current dimensional thermal performance data into a generalised dimensionless framework (incorporating Rayleigh, Nusselt, and Fourier numbers), enabling theoretical comparisons with fundamental fluid dynamics literature.

CRediT authorship contribution statement

Hayder Al-lami: Writing – original draft, Validation, Supervision, Software, Methodology, Investigation, Conceptualization. **Hussain Madhi:** Writing – original draft, Supervision, Formal analysis, Data curation. **Dheyaa S.J. Al-Saedi:** Writing – review & editing, Resources, Project administration, Formal analysis. **Ali A.H. AlMaidi:** Visualization, Resources, Project administration. **Mushtaq A. Al-Furaiji:** Writing – original draft, Methodology, Data curation.

Declaration of competing interest

The authors declare that they have no known competing financial interests or personal relationships that could have appeared to influence the work reported in this paper.

Acknowledgements

The authors disclose no acknowledgements.

Data availability

Data will be made available on request.

References

[1] Q. Al-Yasiri, M. Alktranee, Y. Hamed, A. Aqeel, M. Lafta, P. Bencs, M. Szabo, Experimental analysis on the effect of cavity shape on the thermal and mechanical performance of hollow concrete bricks, Results. Eng. 28 (2025) 108212, https://doi.org/10.1016/J.RINENG.2025.108212.
[2] A.W. Abbood, K.M. Al-Obaidi, H. Awang, A.M.A. Rahman, Achieving energy efficiency through industrialized building system for residential buildings in Iraq, Int. J. Sustain. Built. Environ. 4 (2015) 78–90.
[3] A.M. Reveshti, F.H. Mansoub, J.N. Reveshti, K.F. Bonab, Evaluation of thermal performance of innovative insulation materials for energy-efficient buildings in cold climates, Int. J. Thermofluids 32 (2026) 101544.
[4] S. Hameed, S.A.A. Gillani, M. Tahir, R. Hameed, S. Abbas, M.L. Nehdi, M. Ahmad, Investigating lightweight recycled brick aggregate concrete incorporating EPS beads: application to masonry units, Results. Eng. 25 (2025) 104019.
[5] K. Yadav, A. Singh, O.N. Bhat, R.L. Sharma, Transforming waste into innovation: a review of plastic bricks as sustainable construction materials, Discov. Civ. Eng. 1 (2024) 38.
[6] S.A. Fathi, A.A. Al-Attar, Sustainable concrete with wood ash and recycled clay block aggregate, Misan. J. Eng. Sci. 4 (2025) 103–123.
[7] Q. Al-Yasiri, M. Alktranee, H. Al-Lami, M. Szabó, P. Bencs, Hourly thermal analysis of innovative concrete bricks using sawdust and phase change material, Results. Eng. 29 (2026) 109313, https://doi.org/10.1016/j.rineng.2026.109313.
[8] R. Salman, S. Aljabair, J.M. Jalil, Enhancing thermal performance and energy efficiency in concrete bricks with phase change materials: a numerical study, J. Energy Storage 125 (2025) 116937, https://doi.org/10.1016/J.EST.2025.116937.
[9] J. Zhang, C. Shen, G. Diao, Application and microstructure properties of nanomaterials in new concrete materials, J. Nanomater. 2022 (2022) 7396295.
[10] M. Amin, K. Abu el-Hassan, Effect of using different types of nano materials on mechanical properties of high strength concrete, Constr. Build. Mater. 80 (2015) 116–124.
[11] M.S. Aljibory, B.J. Alsulayfani, M.N. Mahmood, Improvement of concrete mechanical properties by adding nanomaterials, Misan. J. Eng. Sci. 2 (2023) 57–70.
[12] A.M.S. Hassan, A. Abdeen, A.S. Mohamed, B. Elboshy, Thermal performance analysis of clay brick mixed with sludge and agriculture waste, Constr. Build. Mater. 344 (2022) 128267.
[13] D. Mahapatra, V. Madav, A.B.T.P. Setty, Mechanical and dynamic thermal performance evaluation of rice husk blended cement plaster when used with different bricks, J. Build. Eng. 82 (2024) 108120.
[14] T. Kantasiri, P. Kasemsiri, U. Pongsa, P. Posi, P. Chindaprasirt, Optimization of concrete containing waste crumb rubber mix design for thermal insulating applications using Taguchi method, Constr. Build. Mater. 434 (2024) 136636.
[15] M. Nagapan, S.P. Yap, K.H. Mo, B.F. Lau, N.A.M. Rohaizad, Recycling spent mushroom substrate as a partial fine aggregate substitute in cement brick production: evaluating mechanical, durability, and thermal insulation properties, Sustain. Chem. Pharm. 46 (2025) 102050.
[16] M. Gonçalves, A. Figueiredo, G. Vela, F. Rebelo, R.M.S.F. Almeida, M.S.A. Oliveira, R. Vicente, Effect of macrocapsule geometry on PCM performance for thermal regulation in buildings, Energies 18 (2025) 303.
[17] Q. Al-Yasiri, M. Szabó, Experimental study of PCM-enhanced building envelope towards energy-saving and decarbonisation in a severe hot climate, Energy Build. 279 (2023) 112680.
[18] R. Salman, S. Aljabair, J.M. Jalil, Enhancing thermal performance and energy efficiency in concrete bricks with phase change materials: a numerical study, J. Energy Storage 125 (2025) 116937.
[19] Y. Zhang, X. Sun, M.A. Medina, Experimental assessment of concrete masonry units integrated with insulation and phase change material: a wall-pattern study, Energy 289 (2024) 130038.
[20] T.A. Mukram, J. Daniel, Performance evaluation of a novel cement brick filled with micro-PCM used as a thermal energy storage system in building walls, J. Energy Storage 77 (2024) 109910.
[21] Q. Al-Yasiri, M. Szabó, Thermal performance of concrete bricks based phase change material encapsulated by various aluminium containers: an experimental study under Iraqi hot climate conditions, J. Energy Storage 40 (2021) 102710, https://doi.org/10.1016/j.est.2021.102710.
[22] M. Wu, R. Ji, P. Dou, C. Gao, Y. Zhang, J. Zhang, L. Chen, E. Fernandez-Rodriguez, Energy-harvesting performance of twin-rotor vertical-axis wind turbines with phase interference under different solidities, J. Mar. Sci. Eng. 14 (2026) 508.
[23] X. Zhang, R. Ji, K. Sun, J. Zhang, X. Zhang, M. Yin, M. Kong, R. Reabroy, A review of ocean tidal current energy technology: advances, trends, and challenges, Phys. Fluids 37 (2025).
[24] M. Yin, R. Ji, R. Zhu, S. Xu, K. Sun, J. Zhang, Y. Zhang, R. Reabroy, Performance and wake prediction of a ducted tidal stream turbine in yaw misalignment using the lattice Boltzmann method, Energy Convers. Manag. 347 (2026) 120574.
[25] M. Alktranee, Q. Al-Yasiri, K. Saeed Mohammed, H. Al-Lami, P. Bencs, Energy and exergy assessment of a photovoltaic-thermal (PVT) system cooled by single and hybrid nanofluids, Energy Convers. Manag.: X 24 (2024) 100769, https://doi.org/10.1016/j.ecmx.2024.100769.
[26] H. Al-Lami, M.S. Mohammed, R. Ali, A. Alshara, H.K.A. Zahra, Characteristics of heat transfer and turbulent flow in a baffled pipe with different arrangements, Eur. J. Eng. Technol. Res. 7 (2022) 113–119, https://doi.org/10.24018/ejeng.2022.7.6.2921.
[27] A. Sedaghat, M.R. Karami, M. Eslami, Improving Performance of a Photovoltaic Panel by Pin Fins: A Theoretical Analysis, 2020 n.d.
[28] Comparative Study on Different Cooling Techniques for Photovoltaic Thermal management: Hollow fins, Wavy Channel and Insertion of Porous Object with Hybrid Nanofluids, 2023 n.d. https://www.sciencedirect.com/science/article/abs/pii/S1359431123004878.
[29] F. Wang, Z. Li, D. Pang, Z. Li, X. Zhao, X. Cheng, M. Liu, Y. Zhang, W. Guo, Enhancing heat transfer of photovoltaic panels with fins, Int. J. Energy Res. 2024 (2024), https://doi.org/10.1155/2024/5180627.
[30] B. Gay, J.D. Jenkins, N.V. Mackley, Shell-side heat transfer in double-segmentally baffled cylindrical shell-and-tube exchangers, Lett. Heat Mass Transf. 9 (1982) 39–47, https://doi.org/10.1016/0094-4548(82)90046-7.
[31] O. Turgut, E. Kizilirmak, Effects of reynolds number, baffle angle, and baffle distance on 3-D turbulent flow and heat transfer in a circular pipe, Therm. Sci. 19 (2015) 1633–1648, https://doi.org/10.2298/TSCI121011045T.
[32] R. Kumar, A. Kumar, A. Sharma, R. Chauhan, M. Sethi, Experimental study of heat transfer enhancement in a rectangular duct distributed by multi V-perforated baffle of different relative baffle width, Heat Mass Transf./Waerme- Stoffuebertragung 53 (2017) 1289–1304, https://doi.org/10.1007/s00231-016-1901-7.
[33] Al-Lami, D.S.J. Al-Saedi, A.A.H. AlMaidib, Q. Al-Yasiri, Conjoint effect of nanofluids and baffles on a heat exchanger thermal performance: numerical approach, Misan. J. Eng. Sci. 3 (2024) 137–155, https://doi.org/10.61263/mjes.v3i2.105.
[34] H. Al-Lami, K. Saeed Mohammed, A.A.H. AlMaidi, H.K. Abdulzahra, W. T. Alramdhan, Numerical investigation of photovoltaic thermal management using conical, pyramid, and hexagonal fins, Case Stud. Therm. Eng. 77 (2026) 107491, https://doi.org/10.1016/j.csite.2025.107491.
[35] D.S.J. Al-Saedi, H. Al-Lami, M.A. Al-Furaiji, R.A. Hussein, Q. Al-Yasiri, Fin orientation effect on passive cooling of photovoltaic panels: an experimental study under extreme hot climate, Future Technol. 5 (2026) 72–83, https://doi.org/10.55670/fpll.futech.5.1.8.
[36] H. Al-Lami, N.N. Al-Mayyahi, Q. Al-Yasiri, R. Ali, A. Alshara, Performance enhancement of photovoltaic module using finned phase change material panel: an experimental study under Iraq hot climate conditions, Energy Sources A: Recovery Util. Environ. Eff. 44 (2022) 6886–6897, https://doi.org/10.1080/15567036.2022.2103601.
[37] S. Tamna, Numerical heat transfer investigation in a tube with inclined flower baffles, J. Res. Appl. Mech. Eng. 2 (2014), https://doi.org/10.14456/jrame.2014.10.
[38] H. Sousa, I. Gondim, A. Bertini, Changes in Clay Hollow block geometry for energy efficiency benefits-thermal simulation for Brazil, (2023).
[39] S. Vera, C. Figueroa, S. Chubretovic, J.C. Remesar, F. Vargas, Improvement of the thermal performance of hollow clay bricks for structural masonry walls, Constr. Build. Mater. 415 (2024) 135060.
[40] X. Chen, Q. Chun, N. Van Den Bossche, Thermal performance of traditional cavity walls: accounting for complex cavity geometry and bonding variability, Energy Build. 341 (2025) 115816.
[41] S. Ahmad, D. Liu, B.M. Cham, W. Xu, S. Yang, Optimization of heat transfer efficiency of electronic device through conjugate heat transfer using Darcy-Forchheimer modelled base plate: 2D versus 3D computations, Appl. Therm. Eng. 265 (2025) 125535.
[42] A.T. Wijayanta, A localized meshless approach using radial basis functions for conjugate heat transfer problems in a heat exchanger, Int. J. Refrig. 110 (2020) 38–46.

[43] uop [Architecture_Ebook]_Masonry_Design_and_Detailing_For_Architects_and_Contractors-20615_Part279, (n.d.).
[44] Q. Al-Yasiri, M. Szabó, Building envelope-combined phase change material and thermal insulation for energy-effective buildings during harsh summer: simulation-based analysis, Energy Sustain. Dev. 72 (2023) 326–339, https://doi.org/10.1016/J.ESD.2023.01.003.
[45] Z. Svoboda, M. Kubr, Numerical simulation of heat transfer through hollow bricks in the vertical direction, J. Build. Phys. 34 (2011) 325–350.
[46] U. Manual, ANSYS FLUENT 12.0, theory Guide 67 (2009).
[47] Q. Al-Yasiri, M. Szabó, Thermal analysis of concrete bricks-embedded phase change material: a case study under hot weather conditions, Case Stud. Constr. Mater. 18 (2023) e02193, https://doi.org/10.1016/J.CSCM.2023.E02193.
[48] M. Vaughn, ASHRAE research Report: 2017-2018, ASHRAE J. 60 (2018) 73–84.
[49] H.K. Versteeg, W. Malalasekera, The finite volume method, Introd. Comput. Fluid Dyn. 102 (1995).
[50] J.H. Ferziger, M. Perić, R.L. Street, Computational Methods for Fluid Dynamics, Springer, 2002.